arXiv:astro-ph/9804231v1 22 Apr 1998

The circumstellar shell of the post-AGB star HD 56126: the $^{12}C^{12}C/^{12}C^{13}C$ isotope ratio and $^{12}C^{16}O$ column density

Eric J. Bakker[1] and David L. Lambert
Department of Astronomy and W. J. McDonald Observatory, University of Texas, Austin, TX 78712-1083, USA
ebakker@astro.as.utexas.edu, dll@astro.as.utexas.edu

ABSTRACT

We have made the first detection of circumstellar absorption lines of the $^{12}C^{13}C$ $A^1\Pi_u - X^1\Sigma_g^+$ (Phillips) system 1-0 band and the $^{12}C^{16}O$ $X^1\Sigma^+$ first-overtone 2-0 band in the spectrum of the post-AGB star HD 56126 (IRAS 07134+1005). All current detections of circumstellar molecular absorption lines towards HD 56126 ($^{12}C_2$, $^{12}C^{13}C$, $^{12}C^{14}N$, $^{13}C^{14}N$, and $^{12}C^{16}O$) yield the same heliocentric velocity of $v_{\rm CSE} = 77.6 \pm 0.4$ km s^{-1}. The $^{12}C_2$, $^{12}C^{13}C$, and $^{12}C^{16}O$ lines give rotational temperatures and integrated column densities of $T_{\rm rot} = 328 \pm 37$ K, $\log N_{\rm int} = 15.34 \pm 0.10$ cm^{-2}, $T_{\rm rot} = 256 \pm 30$ K, $\log N_{\rm int} = 13.79 \pm 0.12$ cm^{-2}, and $T_{\rm rot} = 51 \pm 37$ K, $\log N_{\rm int} = 18.12 \pm 0.13$ cm^{-2} respectively. The rotational temperatures are lower for molecules with a higher permanent dipole moment. Derived relative column densities ratios are $^{12}C_2/^{12}C^{13}C = 36 \pm 13$, and $^{12}C^{16}O/(^{12}C_2+^{12}C^{13}C) = 606 \pm 230$. Combined with data from Paper III we find relative column densities of $^{12}C^{16}O/(^{12}C^{14}N+^{13}C^{14}N) = 475 \pm 175$ and $^{12}C^{14}N/^{13}C^{14}N = 38 \pm 2$.

Under chemical equilibrium conditions, $^{12}C^{13}C$ is formed twice as easily as $^{12}C_2$. The isotopic exchange reaction for $^{12}C_2$ is too slow to significantly alter the $^{12}C_2/^{12}C^{13}C$ ratio and the $^{12}C_2$ to $^{12}C^{13}C$ ratio a good measure of half the carbon isotope ratio: $^{12}C/^{13}C = 2\times{}^{12}C_2/^{12}C^{13}C = 72 \pm 26$. This is in agreeement with our prediction that the isotopic exchange reaction for $^{12}C^{14}N$ is efficient and our observation in Paper III of $^{12}C^{14}N/^{13}C^{14}N = 38 \pm 2$.

A fit of the C_2 excitation model of van Dishoeck & Black (1982) to the relative population distribution of C_2 yields $n_{\rm c}\sigma/I = 3.3 \pm 1.0 \times 10^{-14}$. At $r \simeq 10^{16}$ cm this translates in $n_{\rm c} = 1.7 \times 10^7$ cm^{-3} and $\dot{M} \simeq 2.5 \times 10^{-4}$ M$_\odot$ yr^{-1}.

Subject headings: line: identification – molecular data – molecular processes – stars: AGB and post-AGB – stars: circumstellar matter– individual stars: HD 56126

1. Introduction

HD 56126 (IRAS 07134+1005) is in the post-AGB stage (also referred to as the Pre-Planetary Nebulae stage) of stellar evolution. This is the relative short transition stage from the Asymptotic Giant Branch (AGB) to the White Dwarf (WD) phase (Iben 1983). Low-mass stars (0.8 M$_\odot \leq$ M$_* \leq$ 8.0 M$_\odot$) may experience up to three dredge-up episodes. The first occurs on the Red Giant Branch (RGB). The second on the Early-AGB (E-AGB) is limited to stars with initial masses in the range of 4 to 8 M$_\odot$. The third occurs on the Thermal Pulsating-AGB (TP-AGB). The last dredge-up changes the surface abundances

[1] present address: TNO-FEL, Electro Optics Group, P.O. Box 96864, 2509 JG, The Hague, The Netherlands, e.j.bakker@fel.tno.nl

of the star most drastically: most noticeable the carbon and s-process elements abundances enhanced (Forestini & Charbonnel 1997). Several studies of the photospheric abundance of post-AGB stars have indeed shown that some of these stars are carbon rich and have enhanced abundances of s-process elements (Luck & Bond 1989; Klochkova 1995; van Winckel 1997; Reddy et al. 1997,1998; Decin et al. 1998). Since AGB stars lose mass through a dense stellar wind, post-AGB stars are surrounded by a shell of material which expands at typically 3 to 30 km s^{-1}. This material constitutes the circumstellar environment (CSE) of the star. The CSE material mixes with interstellar clouds and forms the parent material for the next generation of stars. In this manner, nucleosynthesis products are used to build new stars and the Galaxy is enriched with heavy elements (elements more massive than helium). The study of the chemical structure of the CSE of evolved stars is therefore of importance to understand the chemical enrichment of the Universe.

Stellar evolution theory needs constraints from observations. The $^{12}C/^{13}C$ suits this goal very well since during the AGB evolution ^{12}C is formed in the helium burning layer, while ^{13}C is formed as a by-product in the hydrogen burning layer. The observed ratio of these two isotopes depends on the efficiency and the relative strength of these two layers, and on the efficiency of the dredge-up processes.

Theoretical models of the chemical structure of the CSE of highly evolved stars have mainly concentrated on understanding the well-studied, and well-observed carbon star IRC +10216 (for references see Olofsson 1998). When a star reaches the tip of the AGB, the mass-loss rate has its maximum strength and drops several orders of magnitude after the star leaves the AGB. Material ejected during the AGB phase slowly expands from the star and leaves a cavity in the CSE which will grow with time. Eventually leading to a cavity the size of a planetary nebulae. The elemental composition of the CSE is fixed after the material leaves the surface of the star. In contrast, the molecular composition of the CSE is constantly changing under the influence of the stellar and interstellar radiation fields: molecules are destroyed and formed continuously. Most studies of the CSE make use of molecular line emission in the sub-millimeter and radio (e.g. CO and HCN) while recently the ISO satellite has allowed a study of molecular lines in the infrared. Emission lines of spatially unresolved sources provide no positional information, and only partial velocity information (the radial component). This is obviously not the case for absorption lines since they are formed in a pencil-beam towards the continuum source and probe therefore a well defined region of the CSE. Secondly, a molecular absorption line spectrum has many lines allowing a study of the population of the energy levels of the molecules and processes like optical pumping. Absorption lines therefore yield information additional to that already available from emission line studies. As part of an ongoing effort to study the characteristics of post-AGB stars, we have been studying circumstellar $^{12}C^{14}N$ and $^{12}C_2$ lines in the optical spectra of post-AGB stars (referred to as C2CN stars) which show the unidentified 21 μm feature (Kwok et al. 1989,1995; Hrivnak & Kwok 1991; Justtanont et al. 1996). These electronic bands allow an accurate determination of the expansion velocity of the CSE, rotational temperature, column density, and molecular column density ratios (Bakker et al. 1996b (Paper I), 1997 (Paper II), Bakker & Lambert 1998 (Paper III)).

In Paper III we presented measurements of the ratio $CN/^{13}CN$ (from now on C means ^{12}C, N means ^{14}N, and O means ^{16}O). We found a ratio of 38 ± 2 but argued that the true $C/^{13}C$ ratio is likely closer to 67 owing to the isotopic exchange reaction ($^{13}C^+ + CN \rightleftharpoons C^+ + {}^{13}CN + \Delta E$). In this paper (IV) we present measurements of the $C_2/C^{13}C$ ratio. Combining these two independent isotope ratios allows us to constrain the isotope exchange reaction and give a more accurate determination of the true $C/^{13}C$ ratio in the CSE surrounding HD 56126.

In Sec. 2 we discuss the optical and infrared observations and the source of the data on the equivalent widths used in our analysis. Sec. 3 describes the sources from which we obtained the molecular data (C_2,

$C^{13}C$, and CO). Sec. 4 is the analysis and Sec. 5 the discussion.

2. Observations and equivalent widths

2.1. Optical

Spectra of the C_2 and $C^{13}C$ $A^1\Pi_u - X^1\Sigma_g^+$ (Phillips) system 1-0 band have been obtained using the coudé cross-dispersed echelle spectrograph (Tull et al. 1995) of the 2.7 meter Harlan J. Smith telescope of the W.J. McDonald Observatory (Table 1). During three consecutive nights in January 1998, 36 exposures of each 30 minutes on HD 56126 have been made. Each exposure gives a CCD frame (TK3 with 2048×2048 pixels) with 18 orders, with each order covering almost 19 Å. A log of the observations is presented in Table 1. Each exposure is individually reduced using the echelle package within IRAF: trimmed, scattered light subtracted, flat fielded, orders extracted, and wavelength calibrated. The 36 spectra are combined on an heliocentric wavelength scale, and finally continuum corrected to obtain the co-added spectrum (Fig. 1). The analysis presented is based on this final co-added spectrum. The spectral resolution, $R = \lambda/\delta\lambda = 130\,000$ (0.″6 wide slit), has been determined from the $FWHM$ of the C_2 lines where the intrinsic width is expected to be less than the instrumental width. No ThAr lines are available in the order in which C_2 occurs, but ThAr lines available in other orders give comparable numbers. In order to be able to remove telluric lines and features that result from fringes on the CCD, we observed the hot star β Ori.

An interval 10160-10220 Å was observed that includes the high excitation C_2 lines ($J'' = 4$ to 22) and low-excitation $C^{13}C$ lines ($J'' = 3$ to 9). Equivalent widths (Table 2) were measured in various ways using the tools available in IRAF/SPLOT.

2.2. Infrared

CO $X^1\Sigma^+$ first-overtone 2-0 infrared spectra towards HD 56126 were acquired with the 3.0 meter NASA Infrared Telescope Facility (IRTF) on Mauna Kea, Hawaii, using the single-order cryogenic echelle spectrograph CSHELL (Tokunaga et al. 1990; Greene et al. 1993) (Table 1). Spectra were obtained with a 0.″5 wide slit and $R = \sigma/\delta\sigma = 43\,000$ (Greene & Denault 1994). The recorded spectrum covers about 10 cm^{-1}. HD 56126 was observed at two settings. One for the 0,1,2 J'' levels, and one the 4,5,6 J'' levels. Observations of $J'' = 3$ were not attempted since this line fell together with a strong telluric feature. In order to remove the sky background, the telescope was nodded 10″ east-west between two successive exposures. The hot star HR 2763 (λ Gem) was observed to act as a reference spectrum to remove telluric features and instrumental artifacts.

The infrared data were reduced with IRAF. First two successive frames were subtracted to remove the bias and sky background. The result was divided by the flat field minus dark frame. The spectra were extracted and the wavenumber calibration was made on identified telluric lines using rest wavenumbers from the AFCRL absorption line catalog for basic input data (ATMOS program, using software written by E.N. Grossman), in combination with the atlas of Hinkle et al. (1995).

The resulting spectrum of HD 56126 was divided by that of the hot star and continuum corrected to obtain the final co-added spectrum (Fig. 2). The analysis presented is based on this final co-added spectrum. Equivalent widths (Table 3) were measured in various ways using the tools available in IRAF/SPLOT, and derived column densities are presented in Table 4, and a log of the observations is presented in Table 1.

3. Molecular data

The software program MOLLEY (Paper III) has been modified and expanded to compute the molecular parameters (line position and line strengths) for the C_2 $A^1\Pi_u - X^1\Sigma_g^+$ (Phillips) system bands and the CO $X^1\Sigma^+$ rovibrational bands (and their isotopes). Given the rotational temperature $T_{\rm rot}$, integrated molecular column density $\log N_{\rm int}$, Doppler broadening parameter (b), and spectral resolution $R = \lambda/\delta\lambda = \sigma/\delta\sigma$, a synthetic spectrum can be computed.

3.1. C_2

C_2 wavenumbers are computed from the molecular constants of Marenin & Johnson (1970) and agree very well with the observed wavenumbers by Chauville & Maillard (1977). Wavenumbers for the isotopes were computed using the standard relations for the mass dependence of the various molecular constants (c.f. Bernath 1995) and the molecular constants for C_2. Wavelengths for $C^{13}C$ (Table 2) have been computed from the wavenumbers by Amiot & Verges (1983) as measured by Fourier Spectroscopy. Conversion from wavenumber (cm^{-1} in vacuum) to wavelength (Å in air) was made using the index of refraction of standard air as given by Morton (1991).

C_2 band oscillator strengths for the Phillips system have been determined experimentally, primarily from measurements of the radiative lifetimes of vibrational levels of the $A^1\Pi_u$ state, and estimated theoretically from quantum chemistry calculations. Unfortunately, experiment and theory are not in completely satisfactory agreement, see for example, the review by Lambert et al. (1995).

Calculations appear to have converged upon a consistent set of oscillator strengths and radiative lifetimes. Langhoff et al. (1990) estimate that their predicted radiative lifetimes are accurate to about 5%. A similar accuracy surely applies to the band oscillator strengths. In our study, we combine observations of lines from the four bands 1-0, 2-0, 3-0, and 4-0 for which the predictions are $f_{(1-0)} = 0.00238$ and $f_{(2-0)} = 0.00144$ by Langhoff et al. (1990), $f_{(3-0)} = 0.0006672$ by Langhoff (1996) and $f_{(4-0)} = 0.000271$ by van Dishoeck (1983) (adjusted to the band oscillator strength ratios of Langhoff et al.). Radiative lifetimes from laser pyrolysis and laser-induced fluorescence (Bauer et al. 1985,1986) are appreciably longer than the predicted lifetimes implying experimental oscillator strengths that are much smaller than the above estimates. Recent measurements by a different technique give results closer to the theoretical values: Erman & Iwamae (1995) measure, for example, a lifetime of 7.1 ± 1.1 μs for vibrational level $v' = 4$ for which Langhoff et al.'s prediction is 6.8 μs but measurements of 11.1 ± 1.1 and 10.7 ± 2.0 μs were reported by Bauer et al. (1985) and Bauer et al. (1986) respectively. In light of the consistent theoretical results (see Langhoff et al. for references), Erman & Iwamae's new experiments, and the estimates derived from observations of interstellar C_2 absorption lines (Lambert et al. 1995), we adopt Langhoff et al.'s predictions and their assessment of their accuracy in our analysis.

The adopted method to compute line strengths from the band oscillator strength is extensively discussed in Paper I and II, and we refer the interested reader to that paper for all details. In computing the line strength for the transitions of the isotopes of C_2 (Table 2 and MOLLEY) we assume that the oscillator strength for the $C^{13}C$ band is the same as for the C_2 band. Band heads of $\nu_{(1-0)} = 9854.0247$ cm^{-1} and $\nu_{(2-0)} = 11413.8250$ cm^{-1} have been taken from Chauville & Maillard (1977) and for $\nu_{(3-0)} = 12947.81$ cm^{-1} and $\nu_{(4-0)} = 14459.01$ cm^{-1} from Ballik & Ramsay (1963).

C_2 is a homo-nuclear molecule, while $C^{13}C$ is a hetero-nuclear molecule. For C_2 only even J'' levels

exist ($J'' = 0, 2, 4, 6...$), while odd and even levels exist for $C^{13}C$ ($J'' = 0, 1, 2, 3...$). The electric dipole moment for C_2 is strictly zero and therefore pure rotational electric dipole transitions ($\Delta J = \pm 1$) cannot occur. Electric quadrupole transitions ($\Delta J = \pm 2$) may occur but with an extremely low probability. The $C^{13}C$ molecule has a very weak electric dipole moment from failure of the Born-Oppenheimer approximation and thus pure rotational transitions are permitted, albeit with a low probability. It is important to realize that the absence of an infrared and sub-millimeter spectrum deprives C_2 of a cooling mechanism and the molecule is excited by the stellar and interstellar radiation fields to supra-thermal temperature ($T_{\rm rot} \geq T_{\rm kin}$). $C^{13}C$ on the other hand has a small dipole moment, and may cool. The population distribution for the two molecules, C_2 and $C^{13}C$, is therefore not necessarily the same and the rotational temperature for $C^{13}C$ may be lower than for C_2. By studying these two molecules simultaneously, potentially important information on the conditions within the CSE could be extracted.

3.2. CO

CO wavenumbers are computed from the Dunham coefficients given by Farrenq et al. (1991). Wavenumbers for Table 3 are after Pollock et al. (1983).

Oscillator strength for CO have been computed after Goorvitch & Chackerian (1994a,1994b) which have a band oscillator strength for CO of $f_{(2-0)} = 0.8957 \times 10^{-7}$. Oscillator strength of the 2-0 band determined by Kirby-Docken & Liu (1978) is 85% of that of Goorvitch & Chackerian. This leaves us with an absolute uncertainty of at most 15 % on the adopted $f_{(2-0)}$-value.

4. Analysis

The analysis presented in this paper is based on the spectra listed in Table 1 supplemented with previous data presented in Paper I (C_2), II (C_2), and III (CN and ^{13}CN), and unpublished data for the C_2 4-0 band. Use of this combined set of data assumes that there has been no change of the excitation conditions of the molecules in the interval of a few years.

The identification of the $C^{13}C$ 1-0 and the CO 2-0 bands yield heliocentric velocities of the line forming region of 78.5 ± 0.4 and 78.7 ± 1.1 km s^{-1}. Within the errors, all velocities of circumstellar molecular absorption lines towards HD 56126 (C_2 : 76.6 ± 0.2; $C^{13}C$: 78.5 ± 0.4; CN : 77.5 ± 0.5; ^{13}CN : 76.7 ± 1.8; CO : 78.7 ± 1.1 km s^{-1}) yield the same heliocentric velocity for the CSE of $v_{\rm CSE} = 77.6 \pm 0.4$ km s^{-1} and successively an expansion velocity of $v_{\rm exp} = 8.0 \pm 0.6$ km s^{-1}. The equality of $v_{\rm CSE}$ for the various species suggests that their regions of residence overlap considerably.

4.1. Doppler b-parameter

In order to derive the column density from the equivalent width of a line, one has to take optical depth effects into account. The $C^{13}C$ and the CO lines are weak and optically thin and their derived column densities (Table 4) are practically independent of the adopted b-value. However, many of the C_2 lines are optical thick and an accurate determination of the b-value is required to computed accurate column densities.

Optical depth effects are quantified by the Doppler b-parameter of the line absorption coefficient that determines the extension of the curve of growth beyond the weak-line limit. To determine the shape of the curve of growth and, hence, the b-parameter, lines from a single vibrational band may be treated as a single dataset. Such lines have accurate relative f-values set by the rotational line strengths (Hönl-London factors). Lines from a given lower (J'') level may be combined immediately to form a part of the curve of growth. This curve for the C_2 Phillips bands may consist of up to twelve measured lines: a P, Q, and a R line from each of three 1-0, 2-0, 3-0, and 4-0 bands. This latter step requires that the relative f-values of the three bands be known. Sets of lines from different J'' levels may be combined after determining the ratio of the column densities of the J'' levels or equivalently the rotational excitation temperature.

In Paper III, circumstellar lines of the CN Red system were combined to yield the b-parameter of $b = 0.51 \pm 0.04$ km s^{-1}. The derived CN curve of growth is well definied. Particularly worthy to note is the fact that the line sample for almost every rotational level spans almost the entire range of equivalent width from weak unsaturated lines to saturated lines on the shoulder of the curve of growth. Thanks to this circumstance, the derivation of the b-parameter and the rotational populations are effectively independent and lead to accurate results. Furthermore, the weak ^{13}CN lines may be compared with rather similar weak CN lines of the same rotational levels such that the CN/^{13}CN ratio is independent of the derived b-parameter. The ratio is dependent on the adopted ratio of f-values for the Violet and Red system bands. (The derived b-parameter is dependent on the relative f-values of the CN Red system bands.)

The C_2 Phillips system 1-0, 2-0, 3-0, and 4-0 bands do not provide such a happy selection of lines. Lines from the four bands from a given lower (J'') level do not span a large range in equivalent widths. The line selection does not run from weak to saturated lines. This necessarity means that the b-parameter cannot be determined independently of the rotational population. It should also be noted that, except for limited measurements of the C_2 1-0 lines, the equivalent widths comes from WHT spectra. Comparision for CN lines show that the McDonald spectra provide more accurate equivalent widths then those from the available WHT spectra.

In light of these limitations, we elected to assume that the appropriate b-parameter for C_2 was the well-determined value found for CN. Curves of growth for the individual C_2 bands are shows in Fig. 3 where the column densities are defined using all available lines. This shows clearly that the observed curve of growths of the bands needs to be shifted systematically relative to the theoretical curves. As noted above, this inconsistency between observed and theoretical curves of growth was not found for the CN Red system bands.

Several potential explanations for this problem affecting the C_2 curves of growth have been considered. Could the relative f-values be at fault? If the f-values are considered as the adjustable parameter, the necessary adjustments corresponds to multiplicative factors of 0.62, 0.98, 1.53, and 2.26 for the 1-0, 2-0, 3-0, and 4-0 bands respectively. Recall that the adopted theoretical f-values have been estimated to be accurate to about 5 %. It is instructive to compare relative f-values: the requirement that lines from the four bands be forced to fit a single curve of growth requires ratios of $f_{(2-0)}/f_{(1-0)} = 1.1$ and $f_{(3-0)}/f_{(1-0)} = 0.8$. In contrast, the theoretical estimates of the same ratios are 0.61 and 0.28 from Langhoff et al. with very similar ratios from other theoretical calculations; for example, van Dishoeck's (1983) f-values correspond to the ratios 0.59 and 0.27. Earlier calculations by Theodorakopoulos et al. (1987) calculations give the ratios of 0.64 and 0.31. In general, absolute values of the f-values are more sensitive to the details of a calculation than are ratios of the f-values that depend primarily on the well determined potential energy curves and secondarily on the variations of the electronic transition moment with inter-nuclear separation. In other words, it is not surprising that Theodorakopoulos et al.'s f-values for the 2-0 band is 29 % larger than

Langhoff et al.'s but that the above sets of f-values ratios from the same pair of calculations are identical to within 5-10 %. It is worth noting too that observations of interstellar C_2 lines toward ζ Oph. give the ratio $f_{(2-0)}/f_{(3-0)} = 2.1 \pm 0.4$ (van Dishoeck & Black 1986) in good agreement with the predictions from Langhoff et al. of 2.15, and in sharp disagreement with the ratio of 1.4 from fitting HD 56126's lines to a single curve of growth. Our assessment of the theoretical f-values for the Phillips system is that their uncertainties do *not* allow curves of growth for the individual bands to be shifted as here required.

Could emission affect the equivalent widths? If unresolved emission from the circumstellar shell fills in the absorption provided by C_2 molecules along the line of sight to the star, the theoretical curves of growth for a uniform slab will be inappropriate. If the emission contribution declines in the order 1-0, 2-0, 3-0, and 4-0, the apparent inconsistencies in the column densities could be explained. It is certainly the case that, if the circumstellar shell is spherically symmetric and large with respect to the star, one expects a P-Cygni profile with blue-shifted absorption and emission to the red of the absorption. (Reddy et al. (1998) observed that the circumstellar C_2 Phillips lines of the post-AGB star IRAS 07431+1115 exhibit P-Cygni profiles while Cohen & Kuhi (1977) found that the absorption component of C_2 towards the Egg Nebulae was present in the polarized light (reflected by the nebulae), while the emission component was unpolarized.) Since the expansion velocity is 8.0 km s^{-1}, the emission and absorption would be fully resolved at our resolution such that dilution of the absorption should be very small. Such emission is not seen in our spectra. We conclude that the shell does not meet the conditions of large and/or spherically symmetric. A special geometry must be provided such that emission from regions off the line of sight to the star provide sufficient flux to fill in the lines with the additional proviso that emission not dominate entirely.

Transition probabilities of Phillips system bands do suggest that emission might account for the apparent inconsistencies in the column densities. Branching ratios, $p_{v'-v''}$, for emission from the levels v' of the upper state may be calculated from transition probabilities, $A_{v'-v''}$, given by van Dishoeck (1983). We find that $p_{(1-0)} = 82$ %, that is 82 % of the radiative decays from $v' = 1$ are in the 1-0 band. For the other observed bands, $p_{(2-0)} = 55$ %, $p_{(3-0)} = 28$ %, and $p_{(4-0)} = 12$ %. Emission rates of these bands depend also on the pumping rates from $v'' = 0$ in the $X^1\Sigma_g^+$ state. These rates should be fairly similar to $v' = 1$, 2, 3, and 4. Then, it is apparent that contamination of the absorption lines by emission should be most serious for the 1-0 band and least for the 4-0 band. This is in the correct sense to account for the apparent inconsistencies in the column densities. It follows that, if this is the correct explanation that C_2 bands should also be seen in emission. for example, the 3-1 band is expected to have twice the emission strength of the 3-0 band. We looked for emission of the 3-1 band in the available spectra which cover this region, no such emission (nor absorption) was found to be present. A simpler and stronger argument against the "emission" hypothesis is that no such effects are seen in the CN Red system lines where the run of $p_{v'-v''}$ from 73 % to 7 % for 1-0 to 4-0 is similar to the run for the Phillips bands.

Could the CN b-parameter be inappropriate for C_2? The CN b-parameter is dominated by contributions from small scale turbulence or a velocity gradient. Since CN and C_2 seem likely to reside in similar layers of the shell, it seemed reasonable to suppose that the molecules have the same b-parameter. It is, however, the case that a lower value, $b = 0.31 \pm 0.05$ km s^{-1} put all lines on a single curve of growth whith adoption of the theoretical f-values. We cannot reject this lower b-parameter directly but note (see below) that it gives an unusually high isotopic ratio of $C/^{13}C \geq 300$.

Could the equivalent widths be in error ? A noticeable difference between the CN and C_2 curves of growth is the larger scatter of the latter about the fitted theoretical curve of growth. We suspect that this reflects the fact that the CN equivalent widths are measured of higher resolution and higher signal-to-nose ratio spectra. Then the vast majority of the C_2 lines, in particular, the C_2 1-0 lines are in

a ratter noisy region of the available spectra. Quite possibly, the C_2 lines are subject to systematic errors. One contributing factor may be that the wings of the strongest lines make a significant contribution of the total equivalent width. For circumstellar lines (with a low b-value), the intrinsic spectrum (as observed at infinite spectral resolution) reaches zero intensity in the core of the profile. Line wings are very extended (several times the $FWHM$ of the line) and represent a significant fraction of the column density. These shallow wings are unfortunately very hard to measure and in most cases we did a Gaussian fit on the profile to obtain the equivalent width and assumed that the contribution of the wing is irrelevant. Tests on the difference between a Gaussian and Voigt profile shows indeed that this could account for a part of the inconsistensies. The stronger the line, the more our measured equivalent widths are in error. Unfortunately there is no easy way to measure the line wings unless we obtain additional very high signal-to-noise ratio spectra at very high-resolution ($R \geq 350\,000$).

In conclusion, the inconsistencies in the derived column densities are most likely a result of the fact that we did not take the extended wings of the absorption profiles into account. Hence, for the saturated lines, our measured equivalent widths are too low.

Fig. 3 shows the curve of growth of C_2 Phillips lines towards HD 56126. The f-values for the Phillips bands have been multiplied by 0.62 1-0, 0.98 2-0, 1.53 3-0, and 2.26 4-0 to improve the fit, and the over-plotted curve of growth is for our preferred value of $b = 0.51 \pm 0.05$ km s^{-1}. Two other curve of growth have been over-plotted which have a b-value marking the error bar of our b determination. By changing the relative f-values to obtain consistent column densities, we find that this introduces a shift of b of 0.05 km s^{-1} towards lower b-values. We therefore conclude that our analysis is not severely affected, but that an increased accuracy can only be reached by taking the (presumed) emission component into account.

In deriving C_2 column densities, we suppose that the theoretical f-values and $b = 0.51$ km s^{-1} are correct, and attribute the offset from the theoretical curve of growth to errors affecting the measured equivalent widths. For the latter reason, we give low weight to the strong C_2 1-0 lines.

Column densities (Table 4) for C_2, $C^{13}C$, CN, ^{13}CN, and CO have been computed by means of a curve of growth for $b = 0.51$ km s^{-1} and using the f-values given in Sec. 3.

4.2. Rotational diagram and column densities

A rotational diagram has been constructed, using the f-values given in Sec. 3, for C_2, $C^{13}C$, and CO (Fig. 4) using the column densities presented in Table 4. For a molecule in local thermodynamic equilibrium (LTE) for which the population distribution of its energy levels can be described by a Boltzmann distribution, the rotational diagram is a straight line. The rotational temperature is given by the negative of the inverse of the slope of the line. From previous work (see for details and references Paper I, II, III) we know that C_2 and CN are not in LTE, their rotational diagram are not linear. The curvature for C_2 in Fig. 4 suggests that this molecule is not in LTE. For the other molecules, too few J'' levels are probed to make a similar claim.

To quantify the excitation of the molecule we make a linear fit to the rotational diagram to obtain an effective rotational temperature. We find $T_{\rm rot} = 328 \pm 37$ K, $\log N_{\rm int} = 15.34 \pm 0.10$ cm^{-2}, $T_{\rm rot} = 256 \pm 30$ K, $\log N_{\rm int} = 13.79 \pm 0.12$ cm^{-2}, and $T_{\rm rot} = 51 \pm 37$ K, $\log N_{\rm int} = 18.12 \pm 0.13$ cm^{-2} for C_2, $C^{13}C$, and CO respectively (see also Table 4). The column densities from the observed levels are not always a good measure for the total column densities. This is best demonstrated by looking at $C^{13}C$. With a rotational

temperature of 256 K, the level that is most populated is $J'' = 7$. Since we observed only the Q-Branch with J'' lower than 9, we miss about 50% of the column density. By assuming a constant rotational temperature and extrapolating to the unobserved levels, we can compute the total $C^{13}C$ column density. Another problem is encountered for C_2. Since this molecule is not in LTE, the integrated column density will be different from the total observed column density.

5. Discussion

The rotational temperatures of $C^{13}C$ and CO are well constrained by a linear fit to their rotational curves (Fig. 4). Within the error C_2 can be fitted to the same rotational temperature as $C^{13}C$, but it is clear that the C_2 rotational curve has a depression from a linear curve near $E(J'')/k = 300$ K. For lower energies (lower J''), the curve is steeper which translates in a lower rotational temperature, while for higher energies (higher J''), the curve is flatter which translates in a higher rotational temperature. This effect has been noted before (Paper I, II) and is characteristic for a molecule which is not in LTE and has a rotational temperature in excess of the kinetic temperature of the gas. C_2 is a homo-nuclear molecule and has therefore no permanent dipole moment. Selection rules do not allow rovibrational (infrared) and rotational (sub-millimeter) transitions. The molecule absorbs energy from the infrared to the ultraviolet (the observed molecular bands), but has no strong cooling mechanism. The result is that the molecule is rotationally excited above the kinetic temperature. An overall fit to the curve yields $T_{\rm rot} = 328 \pm 37$ K. $C^{13}C$ has a very small electric dipole moment and very weak allowed rovibrational and rotational transitions allow the molecule to cool. The possibly lower rotational temperature for $C^{13}C$ of $T_{\rm rot} = 256 \pm 30$ K is consistent with this model. CO has a permanent dipole moment (0.1222 Debye, for references see Kirby-Docken & Liu 1977). It can effectively cool by emitting a photon in the infrared or sub-millimeter. It is thus not unexpected that we find a rotational temperature lower than that for C_2 and $C^{13}C$. CN, with a permanent dipole moment of 1.45 ± 0.08 Debye (Thomson & Dalby 1968), cools more efficiently and has a lower rotational temperature of $T_{\rm rot} = 11.5 \pm 0.6$ K. Besides the difference in dipole moment, there are second order factors which should be considered in order to understand the excitation of the molecule. Since each molecules has its own characteristic absorption spectrum, different molecules absorb different parts of the stellar spectrum. The energy distribution of the central stars, the star's photospheric spectrum, and the reddening between the star and the line forming region should therefore be considered. Clearly, it would be of great interest to model the excitation of the five molecules detected and extract information about the conditions within the CSE from their excitation.

Because of the difference in rotational temperature between C_2 and $C^{13}C$, and the fact that $C^{13}C$ has twice as many J'' levels available, the $C_2/C^{13}C$ can not be determined for each J'' level independently. Instead the only acceptable way is by integrating the population over all available levels. The unobserved levels for $C^{13}C$ contain a significant fraction of the total column density and the total $C^{13}C$ column density can therefore only be obtained by computing a rotational temperature and extrapolating to the unobserved energy levels (labeled as $\log N_{\rm int}$ in Table 4). Using the integrated column densities for C_2 and $C^{13}C$ we find $C_2/C^{13}C = 36 \pm 13$.

The conversion from $C_2/C^{13}C$ to $C/^{13}C$ is rather straightforward. Under chemical equilibrium conditions, $C^{13}C$ is formed twice as easily as C_2 (Tatum 1966). This can be best demonstrated with Tatum's example. In a draw there are equal number of white and black socks (^{12}C and ^{13}C atoms to make $C_2H_2 \rightarrow C_2H \rightarrow C_2$). By taking at random two socks out of the draw, the possible combinations are (white,white), (white,black), (black,white), and (black,black). Since (white,black) is the same as

(black,white) the probability is 1:2:1 for a white, mixed, and black pair of socks. Hence the equilibrium abundance of the hetero-nuclear molecule must be twice that of the homo-nuclear molecule. Excluding any other reaction this leads to $C/^{13}C = 2 \times C_2/C^{13}C = 72 \pm 26$.

CN is a polar molecule with a permanent dipole moment. The rate coefficient for the isotopic exchange reaction of CN with C^+ is as high as 10^{-7} cm^{-3} s^{-1} (Adams et al. 1985). Since ^{13}CN has a 31 K lower zero-point energy than CN, the reaction making ^{13}CN from CN is exothermic. In paper III we constructed a simple chemical model of the CSE of HD 56126 and found that for $C_2/^{13}CN = 38 \pm 2$ we get $C/^{13}C \simeq 67$. C_2 is a symmetric molecule possessing no permanent dipole moment, theory predicts a rate coefficient which is typically 10^{-9} cm^{-3} s^{-1}. Since $C^{13}C$ has a 25 K lower zero-point energy than C_2 the reaction making $C^{13}C$ from C_2 is exothermic. Since the zero-point energy difference for $C^{13}C$ and ^{13}CN to C_2 and CN respectively are about the same, and C_2 and CN have about the same abundance with distance from the star, we can use the chemical model of Paper III (their Fig. 6.d.) to assess the importance of the isotopic exchange reaction for C_2. We find that our model predicts $C_2/C^{13}C = 60$ for $C/^{13}C = 67$. Taking into account the many uncertainties of this model (C^+ abundance, kinetic temperature etc.) we argue that within the errors of our computations, the isotopic exchange reaction does not significantly alter the $C_2/C^{13}C$ ratio in the circumstellar shell surrounding HD 56126.

Given these argument for C_2 and CN, we argue that the intrinsic carbon isotope ratio is well constrained by the $C_2/C^{13}C$ ratio as $C/^{13}C = 72 \pm 16$, and that a rate coefficient for the CN isotopic exchange reaction of 10^{-7} cm^{-3} s^{-1} is consistent with the observed $CN/^{13}CN$ ratio.

The prototype of the AGB stars, IRC +10216/CW Leo, is a massive, highly-evolved carbon star with $3M_\odot \leq M_{\rm ZAMS} \leq 5M_\odot$ (Guélin et al. 1995). For IRC +10216 the isotope ratios are well determined and give an estimate of the ratios which one might expect to detect for a carbon-rich post-AGB star like HD 56126: $C/^{13}C = 44^{+3}_{-3}$. (see Forestini & Charbonnel 1997 for an overview). Our estimate of the $C/^{13}C$ ratio for HD 56126's shell is consistent with that of IRC +10216. Results for circumstellar shells around four other carbon stars were provided by Kahane et al. (1992): $C/^{13}C \leq 60$. These too suggest that HD 56126 is not exceptional.

Combining our results from Paper III and this paper yields a column density ratio of $CO/(C_2+C^{13}C) = 606 \pm 230$ and $CO/(CN+^{13}CN) = 475 \pm 175$. These column density ratios do not necessarily reflect abundance density ratios. CO is abundant throughout the whole CSE, while C_2 and CN are only present in a shell within the CSE where interstellar photons photo-dissociate HCN to CN and C_2H_2 via C_2H to C_2 (Cherchneff et al. 1993). Column density ratios of CO to C_2 and CN (excluding their isotopes) have been measured in several ways. Olofsson (1998) lists abundances for a large range of molecules detected in the shell surrounding AGB stars (although most molecules are only detected in IRC +10216). From his work we find $CO/C_2 = 1 \times 10^3$ and $CO/CN = 1 \times 10^3$. Bachiller et al. (1998) present abundance ratios for, among others, CRL 2688 (Egg Nebulae) obtained from sub-millimeter line emission observations CO/CN=909. Within a factor of two these numbers are consistent with what we find for HD 56126. Bachiller et al. suggest that the $CO/^{13}CO \simeq 20$ likely reflects the $C/^{13}C$ for the planetary nebulae. If so, their $C/^{13}C$ is a factor three lower than ours. This could suggest that the objects observed by Bachiller et al. are not the precursors of HD 56126 but possible PN's with higher mass progenitor ($M_* \geq 2$ M$_\odot$) while the progenitor of HD 56126 has ($M_* \leq 2$ M$_\odot$).

A model for the C_2 molecule has been constructed by van Dishoeck & Black (1982) which takes into account collisional and radiative excitation and de-excitation. For $T_{\rm kin} = 25$ K we find $S = n_c\sigma/I = 3.3 \pm 1.0 \times 10^{-14}$ cm^{-1} (see also Bakker et al. 1995). It is curious that these estimates of $T_{\rm kin}$

and S are quite similar to those derived from C_2 molecules in diffuse interstellar clouds. This is surprising as in Paper II we estimated that the circumstellar C_2 molecules are pumped largely by the stellar radiation field. From a fit to the rotational population, $\sigma = 7.8 \times 10^{-16}$ cm^2 as the collisional cross-section for C_2-H_2 (Phillips 1994), and $I(r = 10^{16}\ \mathrm{cm}) \simeq 4.1 \times 10^5$ the ratio of the stellar radiation field relative to the standard interstellar radiation field, we find $n_c = n(H) + n(H_2) = 1.7 \times 10^7$ as the number of collisional partners for C_2. At $r = 10^{16}$ cm this translates in $\dot{M} \simeq 2.5 \times 10^{-4}$ M$_\odot$ yr^{-1}. This mass-loss rate as derived from modeling the C_2 excitation gives a result comparable to the mass-loss rate derived using other techniques.

Based on this work we can make some suggestions to continue this study. A critical detection would be that of the quadrupole transitions of H_2 at 2.2μm and ^{13}CO rovibrational bands at 4.6 μm. This would allow to determine the column density ratio of the detected molecules relative to the most abundant specie (H_2) and the CO/^{13}CO ratio. Secondly, more C2CN stars should be studied to determine the $C_2/C^{13}C$ and $CN/C^{13}N$ ratio to get good statistics. The most ambitious project would be to model the excitation of all molecules simultaneously in order to obtain the physical conditions of the CSE (densities, radiation field, extinction etc.).

The authors acknowledge the support of the National Science Foundation (Grant No. AST-9618414) and the Robert A. Welch Foundation of Houston, Texas. This research has made use of the Simbad database, operated at CDS, Strasbourg, France, the ADS service, and IRAF. We thank the IRTF staff and John Rayner, for their support in obtaining CSHELL spectra.

REFERENCES

Adams, N.G., Smith, D. & Clary, D.C 1985, ApJ 296, L31

Amiot, C. & Verges, J. 1983, A&AS 51, 257

Bachiller, R., Forveille, T., Huggings, P.J. & Cox, P. 1997, A&A 324, 1123

Bakker, E.J., Lamers, H.J.G.L.M., Waters, L.B.F.M. & Schoenmaker, T. 1995, Ap&SS 224, 335

Bakker, E.J., Lambert, D.L. & van Dishoeck, E.F. 1996a, IAU Symposium 177 "The Carbon Star Phenomenon", Ed. Wing, R.F. in press

Bakker, E.J., Waters, L.B.F.M., Lamers, H.J.G.L.M., Trams, N.R. & van der Wolf, F.L.A. 1996b, A&A 310, 893 (Paper I)

Bakker, E.J., van Dishoeck, E.F., Waters, L.B.F.M. & Schoenmaker, T. 1997, A&A 323, 469 (Paper II)

Bakker, E.J. & Lambert, D.L. 1998, ApJ 502, in press (Paper III)

Ballik, E.A. & Ramsay, D.A. 1963, J.Mol.Sp. 137, 84

Bauer, W., Becker, K.H., Hubrick, C., Meuser, R. & Wildt, J. 1985, ApJ 296, 758

Bauer, W., Becker, K.H., Bielefeld, M. & Meuser, R. 1986, Chem.Phys.Lett. 123, 33

Bernath, P.F. 1995, *"Spectra of Atoms and Molecules", Oxford University Press* (New York)

Chauville, J.& Maillard, J.P. 1977, J.Mol.Sp. 68, 399

Cherchneff, I, Glassgold, A.E. & Mamon, G.A. 1993, ApJ 410, 188

Cohen, M. & Kuhi, L.V. 1977, ApJ 213, 79

Decin, L., van Winckel, H., Waelkens, C. & Bakker, E.J. 1998, A&A 332, 928

Erman, P. & Iwamae, A. 1995, ApJ 450, L31

Farrenq, R., Guelachvili, G., Sauval, A.J., Grevesse, N. & Farmer, C.B. 1991, J.Mol.Sp. 149, 375

Forestini, M. & Charbonnel, C. 1997, A&AS 123, 241

Goorvitch, D. & Chackerian, Jr., C. 1994a, ApJS 91, 483

Goorvitch, D. & Chackerian, Jr., C. 1994b, ApJS 92, 311

Greene, T.P., Tokunaga, A.T., Toomey, D.W. & Carr, J.C. 1993, Proc. SPIE 1946, 313

Greene, T.P. & Denault, A. 1994, "CSHELL: NASA IRTF" Cryogenic Echelle Spectrograph, User's Manual, Revision 2.0.1

Guélin, M., Forestini, M., Valiron, P., Ziurys, L.M., Anderson, M.A., Cernicharo, J. & Kahane, C. 1995, A&A 297, 183

Hinkle, K., Wallace, L. & Livingston, W. 1995, "Infrared Atlas of the Arcturus Spectrum, 0.9-5.3 microns", ISBN 1-886733-04-X

Hrivnak, B.J. & Kwok, S. 1991, ApJ 368, 564

Iben, I.Jr. 1983, ARAA 21, 271

Justtanont, K., Barlow, M.J., Skinner, C.J., Roche, P.F., Aitken, D.K. & Smith, C.H. 1996, A&A 309, 612

Kahane, C., Cernicharo, J., Gomez-Gonzalés, J., & Guélin, M. 1992, A&A 256, 235

Kirby-Docken, K. & Liu, B. 1977, J.Chem.Phys. 66, 4309

Kirby-Docken, K. & Liu, B. 1978, ApJS 36, 359

Klochkova, V.G. 1995, MNRAS 272, 710

Kwok, S., Volk, K. & Hrivnak, B.J. 1989, ApJ 345, L5

Kwok, S., Hrivnak, B.J. & Geballe, T.R. 1995, ApJ 454, 394

Lambert, D.L., Sheffer, Y. & Federman, S.R. 1995, ApJ 438, 740

Langhoff, S.R. 1996, Private Communications

Langhoff, S.R., Bauschlicher, Jr., Rendell, A.P. & Komornicki, A. 1990, J.Chem.Phys 92, 3000

Luck, R.E. & Bond, H.E. 1989, ApJ 342, 476

Marenin, I.R. & Johnson, H.R. 1970, JQSRT 10, 305

Morton, D.C. 1991, ApJS 77, 119

Olofsson, H. 1998, Ap&SS 251, 31

Phillips, T.R. 1994, MNRAS 271, 827

Pollock, C.R., Petersen, F.R., Jennings, D.A. & Wells, J.S. 1983, J.Mol.Sp. 99, 357

Reddy, B.E., Parthasarathy, M., Gonzalez, G. & Bakker, E.J. 1997, A&A 328, 331

Reddy, B.E., Bakker, E.J. & Hrivnak, B.J. 1998, A&A in preparation

Tatum, J.B. 1966, Pub.Dom.Ap.Obs.Victoria 13, 1

Theodorakopoulos, G., Petsalakis, I.D., Nicolaides, C.A. & Buenker, R.J. 1987, Chem.Phys. 112, 319

Thomson, R. & Dalby, F.W. 1968, Can.J.Phys. 46, 2815

Tokunaga, A.T., Toomey, D.W., Carr, J.S., Hall, D.N.B. & Epps, H.W. 1990, Proc. SPIE 1235, 131

Tull, R.G., MacQueen, P.J., Sneden, C. & Lambert, D.L. 1995, PASP 107, 251

van Dishoeck, E.F. 1983, Chemical Physics 77, 277

van Dishoeck, E.F. & Black, J.H. 1982, ApJ 258, 533

van Dishoeck, E.F. & Black, J.H. 1986, ApJ 307, 332

van Winckel, H. 1997, A&A 319, 561

This preprint was prepared with the AAS LaTeX macros v4.0.

Table 1: Log of observations of $C^{13}C$ 1-0 and CO 2-0.

Date	HJD^a	Exp. time [s]	λ^b [Å]	SNR	Remark
HD 56126					
10 Jan. 1998	2450823.68	12×1800	8876	20	$C^{13}C$ 1-0 Q-branch
11 Jan. 1998	2450824.68	12×1800	8876	20	$C^{13}C$ 1-0 Q-branch
12 Jan. 1998	2450825.65	12×1800	8876	20	$C^{13}C$ 1-0 Q-branch
β Ori					
10 Jan. 1998	2450823.64	5×200	8876	273	...
11 Jan. 1998	2450824.65	3×200	8876	230	...
co-added HD 56126/β Ori			8876	85	$C^{13}C$ 1-0 Q-branch

Date	HJD^a	Exp. time [s]	σ [cm^{-1}]	SNR	Remark
HD 56126					
22 Feb. 1998	2450866.718	34×300	4281	87	CO 2-0 R(J'')= 4,5,6
23 Feb. 1998	2450867.704	32×300	4266	100	CO 2-0 R(J'')= 0,1,2
HR 2763					
22 Feb. 1998	2450866.770	24×60	4281	163	CO 2-0 R(J'')= 4,5,6
23 Feb. 1998	2450867.756	20×60	4266	711	CO 2-0 R(J'')= 0,1,2
co-added HD 56126/HR 2763			4281	170	CO 2-0 R(J'')= 4,5,6
co-added HD 56126/HR 2763			4266	180	CO 2-0 R(J'')= 0,1,2

[a] heliocentric Julian date of first observation.

[b] central wavelength or wavenumber of relevant order.

Table 2: $C^{13}C$ Phillips system 1-0 band for the transitions with $J'' \leq 9$ (lines are listed in order of increasing wavelength). Derived column densities are given in Table 4.

$B(J'')$	$\lambda_{\rm rest}^{a,b}$ [Å]	$\lambda_{\rm helio}$ [Å]	$f_{J',J''}^{c} \times 10^3$ ±0.1	W_λ [mÅ] ±0.3	Remarks
R(7)	10162.961l	10165.50	0.713	0.6	tentative
R(6)	10163.064l	10165.60	0.731	1.6	tentative
R(8)	10163.297c	10165.70	0.699	2.1	tentative
R(5)	10163.605l	10166.27	0.756	2.2	tentative
R(9)	10164.070l	10166.80	0.688	2.8	tentative
R(4)	10164.583c	...	0.792	...	blended
R(3)	10165.998c	10168.66	0.848	2.7	...
R(2)	10167.851l	...	0.950	...	not detected
R(1)	10170.142c	...	1.187	...	not detected
R(0)	10172.779c	...	2.380	...	not detected
Q(1)	10176.478c	...	1.186	...	not detected
Q(2)	10177.352c	...	1.186	...	blended
Q(3)	10178.665c	10181.33	1.186	4.0	...
Q(4)	10180.412l	10183.08	1.186	5.2	...
Q(5)	10182.598l	10185.24	1.186	2.7	...
P(2)	10183.699c	...	0.237	...	not detected
Q(6)	10185.226l	10187.90	1.185	5.1	...
P(3)	10188.189c	...	0.339	...	not detected
Q(7)	10188.294l	10190.96	1.185	5.0	...
Q(8)	10191.803c	10194.48	1.185	5.5	...
P(4)	10193.123c	...	0.395	...	not detected
Q(9)	10195.751l	10198.39	1.184	4.9	...
P(5)	10198.450c	10201.15	0.431	2.7	tentative
P(6)	10204.313l	...	0.455	...	not observed
P(7)	10210.583l	...	0.473	...	not observed
P(8)	10217.309l	...	0.487	...	not observed
P(9)	10224.469l	...	0.497	...	not observed

[a] wavelengths have been computed from the wavenumbers by Amiot & Verges (1983) and the index of refraction of $n_{\rm air} = 1.0002741$ (Morton 1991).

[b] appended to the wavelength; l: laboratory; c: computed.

[c] computed with $f_{(1-0)} = 0.00238$.

[d] heliocentric velocity of the identified lines $v_{\rm helio} = 78.5 \pm 0.4$ km s^{-1} (excluding tentative and blended lines).

Table 3: CO 2-0 band for transitions with $J'' \leq 9$. Derived column densities are given in Table 4.

$B(\mathrm{J}'')$	$\sigma^{a,b}_{\rm rest}$ [cm^{-1}]	$f^{c}_{J',J''} \times 10^8$	$\sigma^{d}_{\rm obs}$ [cm^{-1}] ± 0.10	$W_\sigma \times 10^3$ [cm^{-1}] ± 0.10	Remarks
R(0)	4263.837l	8.957	4262.45	5.2	...
R(1)	4267.542l	6.007	4266.14	7.1	...
R(2)	4271.177l	5.439	4269.75	8.5	...
R(3)	4274.741l	5.212	...	...	not observed
R(4)	4278.234l	5.098	4276.83	8.7	...
R(5)	4281.657l	5.036	4280.23	5.9	blended
R(6)	4285.009l	5.002	4283.55	3.3	blended
R(7)	4288.290l	4.985	...	...	not observed
R(8)	4291.499l	4.979	...	...	not observed
R(9)	4294.638l	4.981	...	...	not observed

[a] after Pollock et al. (1983).

[b] appended to the wavenumber; l: laboratory.

[c] computed with $f_{(2-0)} = 8.95 \times 10^{-8}$.

[d] heliocentric velocity of the identified lines $v_{\rm helio} = 78.7 \pm 1.1$ km s^{-1} (excluding blended lines).

Table 4: Derived column densities and column density ratios based on a curve of growth analysis for a Doppler broadening parameter of $b = 0.51$ km s^{-1} and the f-values given in Sec. 3.

	C_2		$C^{13}C$		CN		^{13}CN		CO	
J'' or N''	no.[a]	$\log N(J'')$[b] [cm^{-2}]	no.[a]	$\log N(J'')$[b] [cm^{-2}]	no.[a]	$\log N(N'')$[c] [cm^{-2}]	no.[a]	$\log N(N'')$[c] [cm^{-2}]	no.[a]	$\log N(J'')$[b] [cm^{-2}]
0	3	14.05 ± 0.30	0	...	10	14.80 ± 0.17	1	13.22 ± 0.10	1	16.89 ± 0.30
1	...	...	0	...	12	15.05 ± 0.17	2	13.59 ± 0.10	1	17.22 ± 0.30
2	12	14.37 ± 0.36	0	...	17	14.85 ± 0.16	2	13.16 ± 0.10	1	17.37 ± 0.30
3	...	...	2	12.57 ± 0.30	11	14.39 ± 0.13	2	12.44 ± 0.10	0	...
4	6	14.67 ± 0.24	1	12.71 ± 0.30	1	13.78 ± 0.10	0	...	1	17.41 ± 0.30
5	...	...	0	...	1	12.70 ± 0.10	0	...	1	17.20 ± 0.30
6	7	14.38 ± 0.35	1	12.70 ± 0.30	0	...	0	...	1	16.91 ± 0.30
7	...	...	1	12.69 ± 0.30	0	...	0	...	0	...
8	7	14.25 ± 0.29	1	12.73 ± 0.30	0	...	0	...	0	...
9	...	...	1	12.68 ± 0.30	0	...	0	...	0	...
10	9	14.13 ± 0.22	0	...	0	...	0	...	0	...
11	...	...	0	...	0	...	0	...	0	...
12	6	14.22 ± 0.29	0	...	0	...	0	...	0	...
13	...	...	0	...	0	...	0	...	0	...
14	6	14.06 ± 0.23	0	...	0	...	0	...	0	...
15	...	...	0	...	0	...	0	...	0	...
16	4	14.09 ± 0.30	0	...	0	...	0	...	0	...
17	...	...	0	...	0	...	0	...	0	...
18	3	13.87 ± 0.30	0	...	0	...	0	...	0	...
19	...	...	0	...	0	...	0	...	0	...
20	3	13.76 ± 0.30	0	...	0	...	0	...	0	...
21	...	...	0	...	0	...	0	...	0	...
22	3	13.47 ± 0.30	0	...	0	...	0	...	0	...
23	...	...	0	...	0	...	0	...	0	...
24	2	13.44 ± 0.30	0	...	0	...	0	...	0	...
$\log N_{\rm obs}^{d}$	71	15.29 ± 0.10	7	13.46 ± 0.12	52	15.44 ± 0.09	7	13.86 ± 0.06	5	17.99 ± 0.13
$\log N_{\rm int}^{e}$		15.34 ± 0.10		13.79 ± 0.12		15.44 ± 0.06		13.86 ± 0.09		18.12 ± 0.13
$T_{\rm rot}$ [K]		328 ± 37		256 ± 30		11.5 ± 0.2		8.0 ± 0.6		51 ± 37

$C_2/C^{13}C$[f]	36 ± 13
$CN/^{13}CN$[f]	38 ± 2
$C/^{13}C$[f]	72 ± 16
$CO/(C_2+C^{13}C)$[f]	606 ± 230
$CO/(CN+^{13}CN)$[f]	475 ± 175

[a] number of lines used in averaging.

[b] if less than 5 lines used, then error is 0.30 dex.

[c] from Paper III.

[d] summed over all observed transitions [cm^{-1}].

[e] integrated using the rotational diagram and an infinite number of transitions [cm^{-1}].

[f] column density ratios derived from $\log N_{\rm int}$.

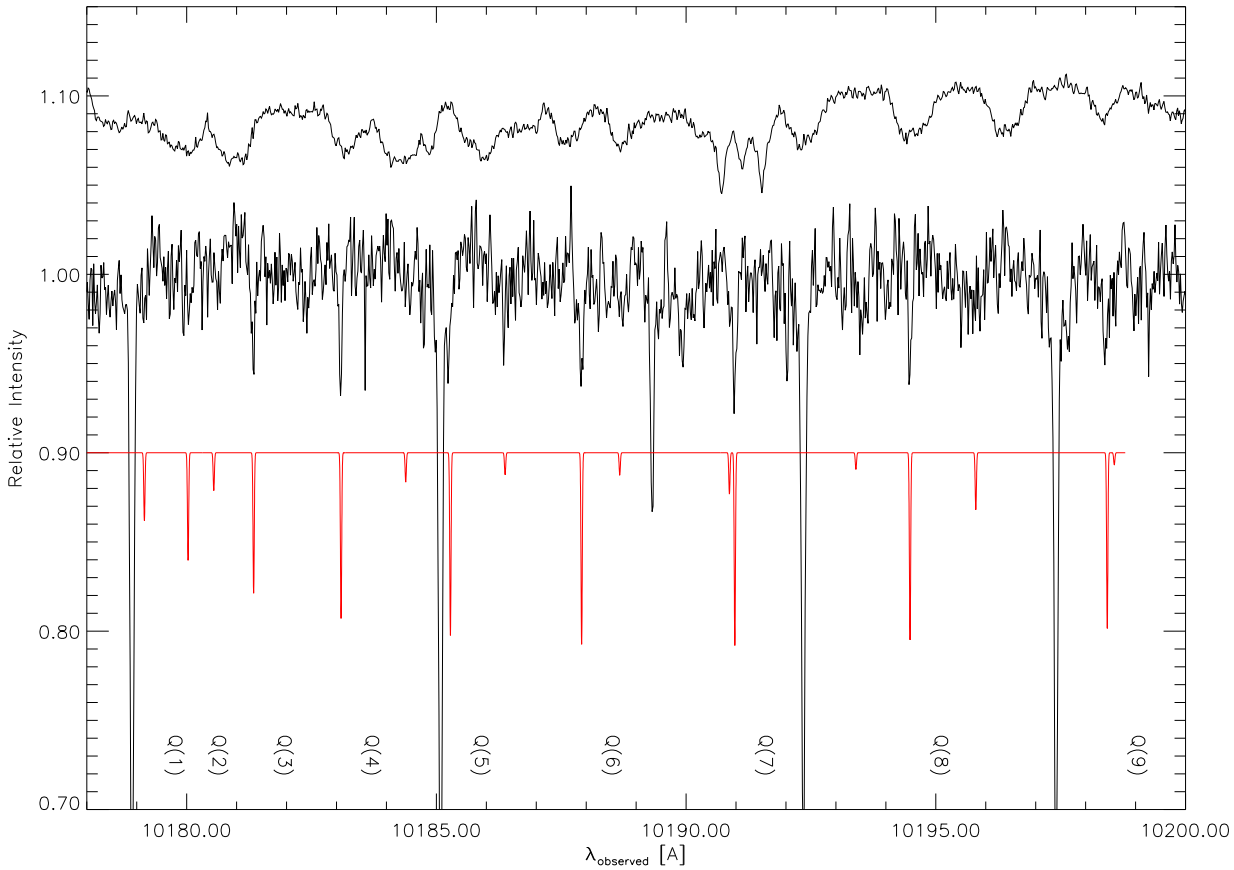

Fig. 1.— $C^{13}C$ Phillips system 1-0 band towards HD 56126. The spectrum of β Ori has been over plotted such that artifacts (telluric features, fringes etc.) are aligned in both spectra. The solid spectrum is the synthetic spectrum ($T_{\rm rot}$ = 256 K, $\log N_{\rm int}$ = 13.79 cm^{-2}, and b = 0.51 km s^{-1}) convolved to a spectral resolution of R = 130 000. The $f_{(1-0)}$-value has been multiplied by 0.62 to obtain a better fit (see Sec. 4.1 for details). The five strong lines which are not identified as $C^{13}C$ are from C_2 1-0 (P(6), Q(12), R(22), P(8), and Q(14)). For clarity, only the Q-branch lines are marked, but the synthetic spectrum is based on all allowed transitions.

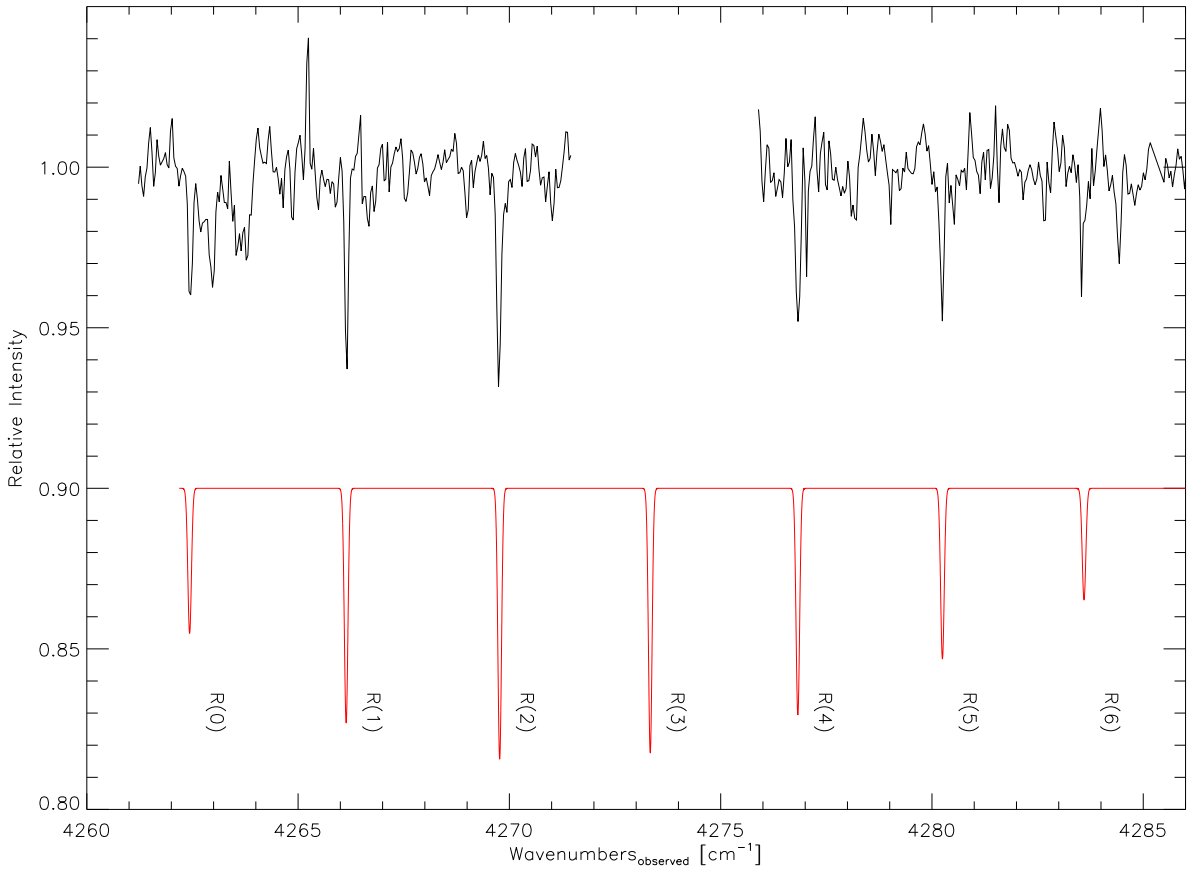

Fig. 2.— CO first overtone band towards HD 56126. The solid spectrum is the synthetic spectrum ($T_{\rm rot} = 51$ K, $\log N_{\rm int} = 18.12$ cm^{-2}, and $b = 0.51$ km s^{-1}) convolved to a spectral resolution of R=43 000. The R-branch lines have been labeled. R(3) was not observed as it was blended by a strong telluric line.

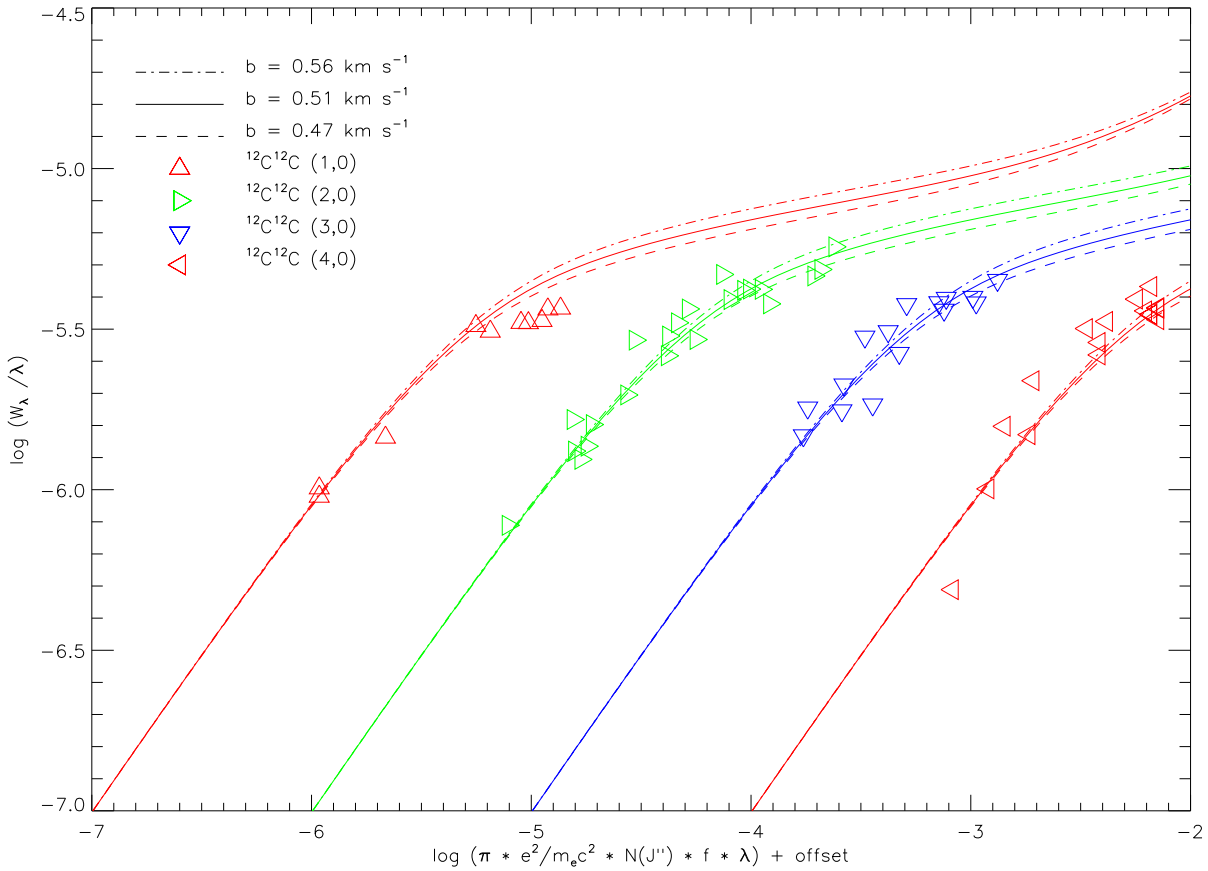

Fig. 3.— Curve of growth for $b = 0.51$ km s^{-1} and the column densities of Table 4. The C_2 data points are labeled with an open triangle (1-0 up; 2-0 right; 3-0 down; 4-0 left). The C_2 bands are offset by multiples of 1 dex in the x-direction. The f-values have been multiplied by 0.62 1-0, 0.98 2-0, 1.53 3-0, and 2.26 4-0 to obtain an improved fit (for details see Sec. 4.1).

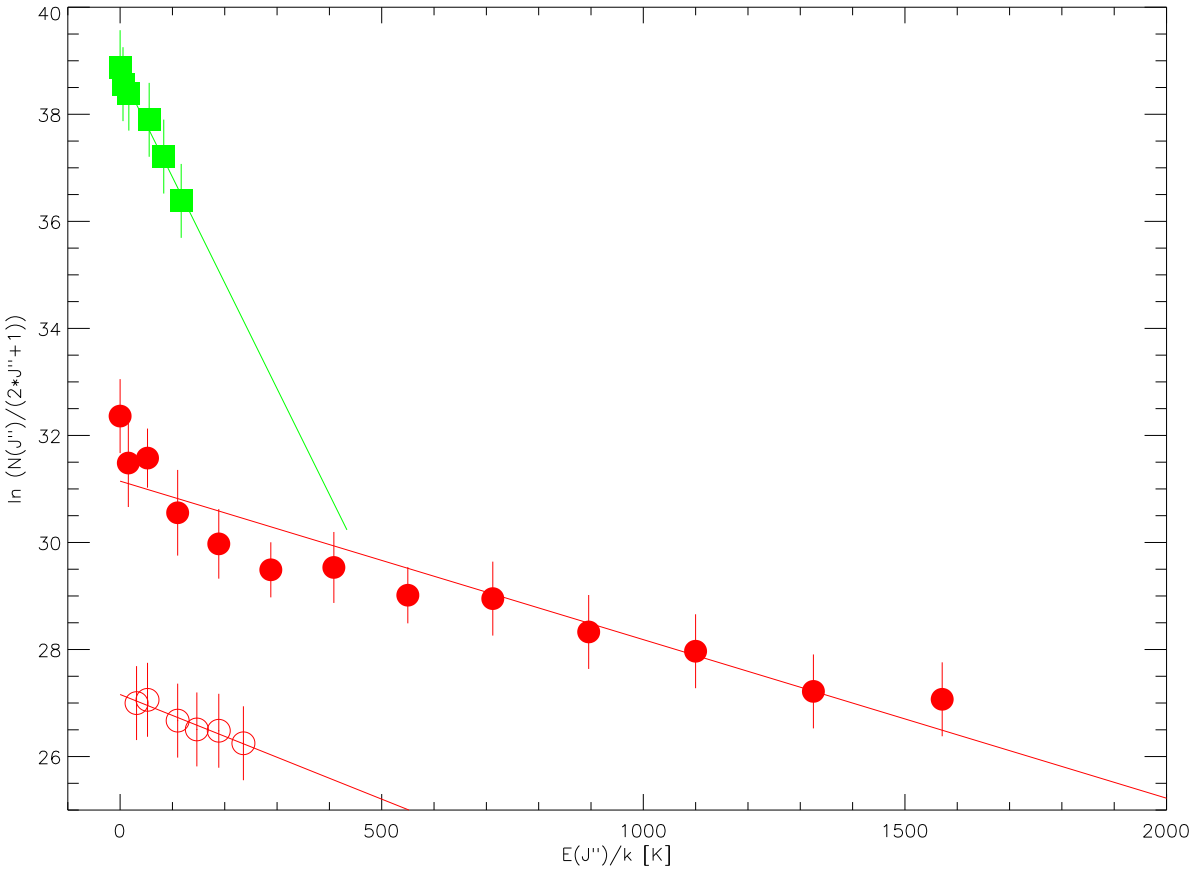

Fig. 4.— Rotational diagram for C_2 (filled circles) and $C^{13}C$ (open circles) Phillips system bands, and the CO (filled squares) first-overtone band towards HD 56126. Column densities and errors used are listed in Table 4. Note that the curvature for the C_2 data points is real and is attributed to non-LTE effects.